LIMIT STRENGTH OF SANDWICH PIPES FILLED WITH STEEL FIBER REINFORCED CONCRETE

C. An, chen@lts.coppe.ufrj.br
X. Castello, xavier@lts.coppe.ufrj.br
S. F. Estefen, segen@lts.coppe.ufrj.br
Ocean Engineering Program, COPPE, Universidade Federal do Rio de Janeiro, CP 68508, Rio de Janeiro, 21941-972, Brazil

Abstract. *Sandwich Pipe (SP) can be an effective solution for the ultra-deepwater submarine pipeline, combining high structural resistance with thermal insulation. Besides polymer, steel fiber reinforced concrete (SFRC) can be another choice for the annular material, based on the characteristics of high fracture toughness and good adhesion with metal. The purpose of this work was to investigate numerically the limit strength of SP with SFRC under external pressure and longitudinal bending. The mechanical behaviors of SFRC with different fiber content were simulated using a damaged plasticity model whose parameters were estimated by the tension and compression tests, and the results showed good correlation between the measured and calculated values. The pressure-curvature ultimate strength for SPs filled with different fiber-content SFRC was presented. Besides, the damage characteristics of SFRC in SPs was also illustrated. In addition, a parametric study was performed in order to investigate the effect of the thickness of each layer on the pressure-curvature collapse envelopes of the SPs.*

Keywords: *sandwich pipes, limit strength, adhesion, damaged plasticity model, steel fiber reinforced concrete*

1. INTRODUCTION

SP is a composite structure consisting of two concentric steel tubes and a polymeric or cement-based core, whose structural resistance and thermal insulation performance have been extensively studied due to their application as an effective solution for the ultra-deepwater submarine pipelines and risers (Estefen *et al.*, 2005). Recently, Castello and Estefen (2007) analyzed numerically the ultimate strength of SP filled with solid polypropylene under external pressure and longitudinal bending, estimated the reeling effect on the ultimate strength and observed that the ultimate strength is strongly dependent on the inter-layer adhesion by performing the numerical simulation with a contact surface model. Extending previous work, Castello and Estefen (2008) conducted the collapse simulation of three SPs employing different annular materials (solid polypropylene, epoxy foam and polyimide foam) and showed that both steel weight and submerged weight are reasonably lighter than a pipe-in-pipe (PIP) system when designed for a hypothetic oil field with the specific requirements, such as inner diameter, maximum heat transfer coefficient and water depth. In another study, Castello *et al.* (2009) investigated the effects of relative ovality direction and temperature-dependent polymer stiffness on the collapse mode. Moreover, Arjomandi and Taheri (2010) presented an analytical approach for estimating the elastic buckling capacity of sandwich pipes with different inter-layer bonding configurations under external hydrostatic pressure. Arjomandi and Taheri (2011) studied the influence of certain structural parameters on the plastic buckling pressure capacity of sandwich pipelines based on the finite element approach and presented an optimization procedure on the material and geometry of the SP system to minimize a desired cost function. Besides, Su *et al.* (2005) studied the transient heat transfer in sandwich pipelines with active electrical heating and showed that SP with active heating is a viable solution to meet severe flow assurance requirements of ultra-deepwater oil production even under unplanned and prolonged cool-down conditions.

Based on the philosophy of the annular materials selection for SP, viz. low cost materials with high compression strength (Estefen *et al.*, 2005), cement-based material can be also adopted. This double skin sandwich structure was firstly introduced as a new form of construction for deep water vessels to resist external pressure (Montague, 1978; Goode *et al.*, 1996), then used for submerged tube highway tunnel (Wright *et al.*, 1991a,b), legs of offshore platforms (Wei *et al.*, 1995a,b) and high-rise bridge piers (Yagishita *et al.*, 2000). With the advantages of enhanced global and local stability, lighter weight, good damping characteristics and good cyclic performance (Elchalakani *et al.*, 2002), a similar concept, concrete-filled double skin steel tubular (CFDST) columns, has been widely investigated for its potential application in building structures. Zhao *et al.* (2002) developed a plastic mechanism to predict the collapse behavior of concrete-filled double-skin stub columns, where confinement and strength degradation were considered for the concrete model. Based on eight compression tests, Elchalakani *et al.* (2002) presented the typical failure modes and a axial strength model for CFDST stub columns with circular hollow sections (CHS) as outer tubes and square hollow sections (SHS) as inner tubes. Han *et al.* (2004) performed a series of compression and bending tests on CFDST stub columns, beams and beam-columns with SHS as outer tubes and CHS as inner tubes, and also developed mechanics models using the unified theory, where a confinement factor was introduced to describe the composite action between the steel tube and the sandwiched

concrete. As a continuation of their research, CFDST stub columns and beam-columns with CHS for both outer and inner tubes were experimentally studied by Tao *et al.* (2004). Furthermore, Han *et al.* (2009) suggested simplified models for the moment versus curvature response and the lateral load versus lateral deflection, respectively, based on the mechanics model predicting the behaviors of CFDST beam-columns subjected to constant axial load and cyclically increasing flexural loading.

In addition to experiments and analytical modeling, the finite element (FE) method have been employed to predict the three-dimensional behaviors of concrete-filled double skin tubes. With an equivalent stress-strain model presented by Han *et al.* (2007), where the study for the torsional behaviors of concrete-filled steel tubes was performed using ABAQUS software, Huang *et al.* (2010) reported a finite element analysis of the compressive behavior of CFDST stub columns with SHS or CHS outer tube and CHS inner tube. To understand the non-uniformly confined concrete by fiber reinforced polymer, Yu *et al.* (2010a) critically assessed the existing Drucker-Prager (D-P) type concrete plasticity models for confined concrete, proposed a modified D-P type model implemented in FE program ABAQUS by modifying its Extended Drucker-Prager Model and making use of the facility of user-defined solution-dependent field variables (SDFV). The proposed model is unable to simulate the reduction of elastic stiffness during the loading process. To overcome the limitation, Yu *et al.* (2010b) developed an improved plastic-damage model within the theoretical framework of the Concrete Damaged Plasticity Model (CDPM) in ABAQUS, which can be exploited in FE models to investigate the behaviors of confined concrete in various forms of columns.

In this paper, the limit strength of sandwich pipes for combined external pressure and longitudinal bending is studied using a finite element (FE) modeling based on commercial FE package, ABAQUS/Standard (6.9-1). Steel fiber reinforced concrete (SFRC) is proposed herein as the core material, since this cementitious composite possesses increased extensibility and tensile strength under flexural loading, as a result of its superior resistance to cracking and crack propagation (Balaguru and Shah, 1992; Holschemacher *et al.*, 2010). The material properties of SFRC used in the FE modeling are adopted from a recent evaluation by Velasco (2008), where a systematic study was performed on the mechanical characteristics of the self-consolidating concrete reinforced with high volumetric fractions of steel fibers. The CDPM is used to simulate the inelastic behavior of damaged SFRC including stiffness degradation and crack opening. The effect of fiber volume fraction on the bending behavior of sandwich pipes are then evaluated. Finally, the pressure-curvature collapse envelopes are presented through the numerical evaluation of the ultimate strength of different geometries of sandwich pipes under combined external pressure and longitudinal bending.

2. FE MODEL FOR EXTERNAL PRESSURE AND BENDING

The same geometrical properties of the sandwich pipes analyzed by Castello and Estefen (2007) are employed in this work, as presented in Table 1, where D_n, t, R_i and R_e present the nominal diameter, the pipe thickness, the inner and outer radius, respectively. Initial ovality ($\Delta_0 = 1\%$) is introduced in the numerical model.

Table 1. Geometrical properties of the sandwich pipes.

D_n (in)	R_i (mm)	R_e (mm)	t (mm)
$6\frac{5}{8}$	77.75	84.15	6.4
Annular	84.15	103.15	19
$8\frac{5}{8}$	103.15	109.55	6.4

2.1 Material characteristics

API X-60 steel was used for inner and outer pipes, with yield stress 414 MPa, Poisson coefficient 0.3 and Young modulus 205 GPa. It was modeled by elasticity theory with Hooke's law and plasticity theory of potential flow rule J2 associated with Von Mises yielding criteria and isotropic hardening for the combined loading models.

The concrete damaged plasticity model defined in ABAQUS/Standard (6.9-1) is used to simulate the mechanical properties of the geopolymer cement, which represents the inelastic behavior with the concepts of isotropic damaged elasticity in combination with isotropic tensile and compressive plasticity. The stress-strain relations for the general three-dimensional multiaxial condition are governed by the scalar damage elasticity equation:

$$\boldsymbol{\sigma} = (1-d)\mathbf{D}_0^{el} : (\boldsymbol{\varepsilon} - \boldsymbol{\varepsilon}^{pl}) = \mathbf{D}^{el} : (\boldsymbol{\varepsilon} - \boldsymbol{\varepsilon}^{pl}) \tag{1}$$

where $\mathbf{D}_0^{el}$ is the initial elastic stiffness of the material, $\mathbf{D}^{el}$ the scalar stiffness degraded elastic stiffness and d the scalar stiffness degradation variable, varying from zero to one. In terms of effective stresses, the yield function takes the form

$$F = \frac{1}{1-\alpha}\left(\bar{q} - 3\alpha\bar{p} + \beta(\tilde{\varepsilon}^{pl})\langle\hat{\bar{\sigma}}_{max}\rangle - \gamma\langle-\hat{\bar{\sigma}}_{max}\rangle\right) - \bar{\sigma}_c(\tilde{\varepsilon}_c^{pl}) = 0 \tag{2}$$

with α and γ are dimensionless material constants, $\beta = (1-\alpha)\bar{\sigma}_c(\tilde{\varepsilon}_c^{pl})/\bar{\sigma}_t(\tilde{\varepsilon}_t^{pl}) - (1+\alpha)$, $\hat{\bar{\sigma}}_{max}$ the maximum principal effective stress, $\bar{p} = -\frac{1}{3}\text{trace}(\bar{\boldsymbol{\sigma}})$ the hydrostatic pressure stress, $\bar{q} = \sqrt{\frac{3}{2}(\bar{\mathbf{S}} : \bar{\mathbf{S}})}$ the Mises equivalent effective stress, $\bar{\mathbf{S}}$ the effective stress deviator.

The damaged plasticity model assumes nonassociated potential plastic flow, $d\varepsilon^{pl} = d\lambda\frac{\partial G(\sigma)}{\partial \sigma}$. The flow potential G used for the model is the Drucker-Prager hyperbolic function, $G = \sqrt{(\epsilon\sigma_{t0}\text{tan}\psi)^2 + \bar{q}^2} - \bar{p}\text{tan}\psi$, where ψ is the dilation angle measured in the $p-q$ plane at high confining pressure, σ_{t0} the uniaxial tensile stress at failure and ϵ is a parameter, referred to as the eccentricity, that defines the rate at which the function approaches the asymptote (the flow potential tends to a straight line as the eccentricity tends to zero). In this work, the dilation angle $\psi = \frac{2}{3}\phi$ is adopted, where ϕ is the internal-friction angle as a critical parameter of the Mohr-Coulomb failure criterion model and can be measured from triaxial compression test.

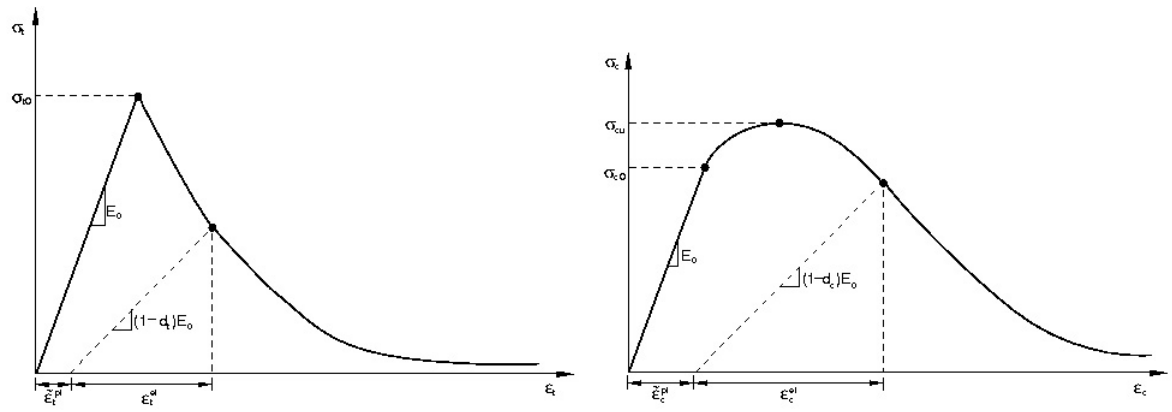

(a) Uniaxial compression (b) Uniaxial tension

Figure 1. Stress-strain curve of the concrete under uniaxial stress

The stress-strain curves for uniaxial tension and compression are needed for defining elastic, plastic and damage behavior, as shown in Fig. 1, where E_0 is the initial (undamaged) elastic stiffness of the material, $\tilde{\varepsilon}_t^{pl}$ and $\tilde{\varepsilon}_c^{pl}$ the tensile and compressive equivalent plastic strains, respectively, d_t and d_c the uniaxial damage variables for tension and compression, respectively, σ_{t0} the uniaxial tensile stress at failure, σ_{c0} the initial compressive yield stress and σ_{cu} the ultimate compressive stress. The stress-strain relations under uniaxial tension and compression loading are

$$\sigma_t = (1-d_t)E_0(\varepsilon_t - \tilde{\varepsilon}_t^{pl}) \tag{3}$$

$$\sigma_c = (1-d_c)E_0(\varepsilon_c - \tilde{\varepsilon}_c^{pl}) \tag{4}$$

The equivalent stress-strain behaviors of tension and compression are presented by the following ideal models modified from Velasco (2008), which are also suitable for the input of damaged plasticity model in ABAQUS/Standard (6.9-1). The tension behavior of SFRC is defined by two curves, including one stress-strain curve before crack nucleation and another postfailure stress-cracking displacement curve, illustrated in Fig. 2. The linear stress-strain relationship is expressed by $\sigma_t(\varepsilon_t) = E_0\varepsilon_t$, $\varepsilon_t \leq \varepsilon_{t0}$ and the tri-linear model for stress-cracking displacement is determined by the following points, $(0, \sigma_{to})$, (w_1, σ_{t1}), (w_2, σ_{t2}) and $(w_u, 0)$, where $\sigma_{t1} = k_1\sigma_{t0}$, $\sigma_{t2} = k_2\sigma_{t0}$, $w_1 = w_u/c_1$ and $w_2 = w_u/c_2$. k_1 and k_2 are the empirical parameters that can better describe the postfailure softening behavior in uniaxial tension tests, while c_1 and c_2 are the constants, $c_1 = 20$ and $c_2 = 5$, respectively.

By extending the definition in Velasco (2008), the stress-strain curve under compression for damaged plasticity model is composed by three sections: a) initial elastic branch, b) damage-based plastic rising branch and c) damage-based plastic declining branch, illustrated in Fig. 3, and the relations are given by the following equations:

$$\sigma_c(\varepsilon_c) = \begin{cases} E_0\varepsilon_c, & \text{for } \varepsilon_c \leq \varepsilon_{c0}, \\ \sigma_{cu}\left[1 - \left(1 - \dfrac{\varepsilon_c}{\varepsilon_{cu}}\right)^{\eta_1}\right], & \text{for } \varepsilon_{c0} < \varepsilon_c \leq \varepsilon_{cu}, \\ \sigma_{cu}\left[1 - \left(\dfrac{\varepsilon_c - \varepsilon_{cu}}{\varepsilon_{cm} - \varepsilon_{cu}}\right)^{\eta_2}\right], & \text{for } \varepsilon_{cu} < \varepsilon_c \leq \varepsilon_{cm}, \end{cases} \tag{5a,b,c}$$

where ε_{cu} is the strain corresponding to the ultimate stress, $\varepsilon_{c0} = \frac{1}{2}\varepsilon_{cu}$, $\varepsilon_{cm} = k_c\varepsilon_{cu}$ the maximum strain in the ideal model, k_c the empirical parameter obtained from the compression tests, η_1 and η_2 the exponentials describing the curvatures of rising and declining branches, respectively. η_1 and η_2 can be determined by $(\varepsilon_{c0}, \sigma_{c0})$ and $(\varepsilon_{c1}, \sigma_{c1})$, where $\varepsilon_{c1} = \frac{3}{2}\varepsilon_{cu}$, σ_{c0} and σ_{c1} are evaluated from the compression test curves.

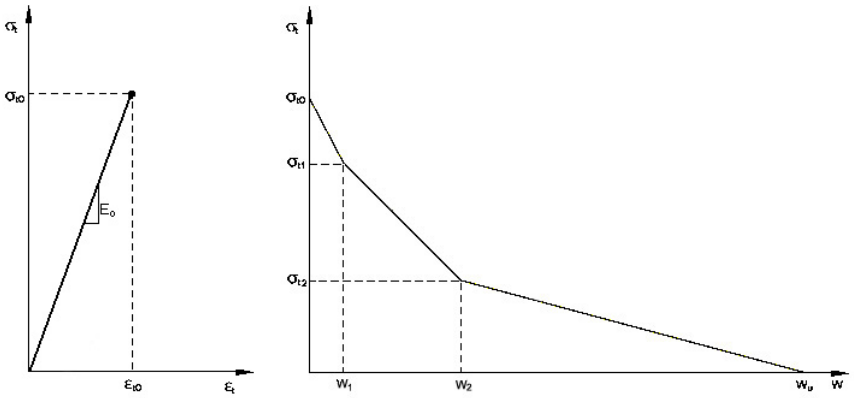

(a) Before crack nucleation (b) Postfailure

Figure 2. Ideal models for the tension behavior of SFRC

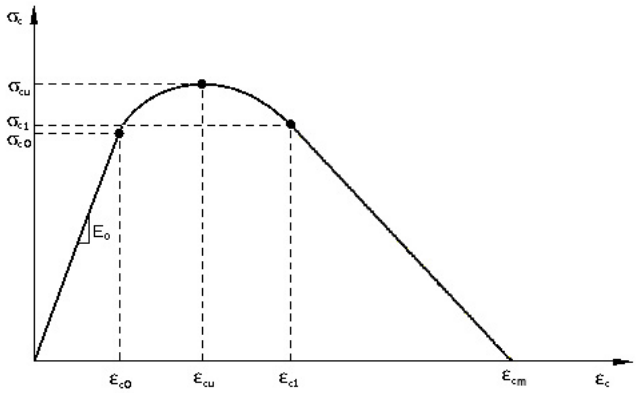

Figure 3. Ideal stress-strain curve in compression.

The damage parameters d_t and d_c need to be calibrated through uniaxial tension and compression tests. Based on the observation and verification on the simulation examples in ABAQUS/Standard (6.9-1), Wang and Chen (2006) concluded that there is a first-order decay exponential function relationship between normalized compressive damage variable D_{cnorm} and normalized compressive inelastic strain $\tilde{\varepsilon}^{in}_{cnorm}$, as follows:

$$D_{cnorm} = A_0 e^{-\tilde{\varepsilon}^{in}_{cnorm}/t_0} + B_0 \tag{6}$$

where $D_{cnorm} = d_c$, $\tilde{\varepsilon}^{in}_{cnorm} = \frac{\tilde{\varepsilon}^{in}_c}{\varepsilon_{cm}}$, $\tilde{\varepsilon}^{in}_c = \varepsilon_c - \frac{\sigma_c}{E_0}$, $A_0 = \frac{1}{e^{-1/t_0}-1}$, $B_0 = -\frac{1}{e^{-1/t_0}-1}$, and the only unknown is t_0. The stress-strain curves are obtained by simulating the uniaxial compression test with various values of t_0 in Abaqus, then the actual value of t_0 can be determined by the agreement with the stress-strain curve from the tests. Similarly, the relationship between normalized tensile damage variable D_{tnorm} and normalized cracking displacement w_{norm} can be also fit with a first-order decay exponential function as follows:

$$D_{tnorm} = A_1 e^{-w_{tnorm}/t_1} + B_1 \tag{7}$$

where $D_{tnorm} = d_t$, $w_{tnorm} = \frac{w}{w_u}$, $A_1 = \frac{1}{e^{-1/t_1}-1}$, $B_1 = -\frac{1}{e^{-1/t_1}-1}$, and the only unknown is t_1. With the determined parameter t_0, the simulation of four-point bending test needs to be performed to calibrate the value of t_1 by correlating the load-displacement curve.

The values of the variables t_0 and t_1 for compression and tension damages, and material properties of SFRC are listed in Tables 2 and 3, where SFRC10, SFRC15 and SFRC20 represent SFRC with fiber content of 1%, 1.5% and 2%, respectively. The Poisson's ratio ν is set to 0.2 for all kinds of SFRC, based on the observation by Thomas and Ramaswamy (2007) that the effect of steel fibers on the Poisson's ratio of concrete was not significant. The internal-friction angle ϕ can be adopted as $37°$, since a trivial effect of the steel fiber reinforcement on this parameter was found by Lu and Hsu (2006). Besides, a small value for the viscosity parameter ($\mu = 0.0001$) is defined to improve the convergence rate in the concrete softening and stiffness degradation regimes, following the suggestion from Barth and Wu (2006). Fig. 4 shows the comparisons between numerical results predicted by Abaqus 6.9-1 and experimental data measured by Velasco (2008) for the axial compression test and four-point bending test of SFRC20. Good agreement

can be found for the compression behavior with the peak force value calculated being only 2.33% greater than the one obtained from the test, while the correlation of the results for the bending behavior is bad, indicating that more efforts are needed to improve the numerical model.

Table 2. Values of the parameters t_0 and t_1 for compression and tension damages used to simulate the SFRC with different percentage of fibers in Abaqus.

Damage parameters	SFRC10	SFRC15	SFRC20
t_0	0.8	0.8	1.1
t_1	0.5	0.7	0.8

Table 3. Material properties of SFRC

Parameters	SFRC10	SFRC15	SFRC20
Young's modulus E(GPa)	28.06	31.48	30.56
Initial compressive yield stress σ_{c0}(MPa)	47.1	48.2	55.0
Compressive yield stress σ_{cu}(MPa)	61.5	70.4	72.5
Tensile yield stress σ_{t0}(MPa)	5.13	5.15	5.20

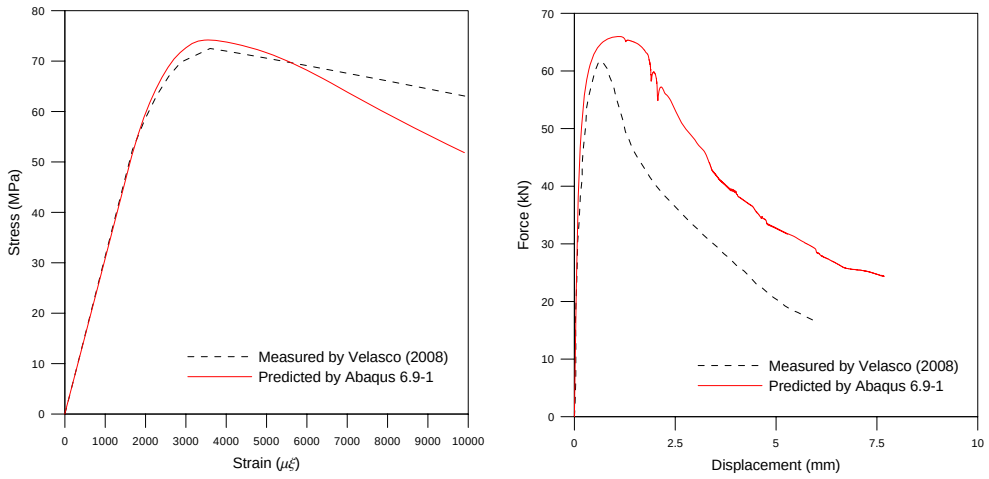

(a) Axial compression test (b) Four-point bending test

Figure 4. Comparison between numerical results predicted by Abaqus 6.9-1 and experimental data measured by Velasco (2008) for the axial compression test and four-point bending test of SFRC20

2.2 Element type and mesh generation

ABAQUS C3D8R continuum-brick elements are used for modeling both the steel tubes and the SFRC core, which can be used for linear analysis and for complex nonlinear analyses involving contact, plasticity and large deformations (Kim and Kuwamura, 2007). Two solid elements are employed for each steel layer and four solid elements are defined for the SFRC annular through the sandwich pipes thickness, and 40 elements are used in the circumferential direction, as shown in Fig. 5.

2.3 Load and boundary condition

Longitudinal and transversal symmetry conditions are assumed for the SPs subjected to combined external pressure and bending moment. The interface condition between steel tubes and SFRC is defined by a "hard" contact model in the normal direction and a frictionless interaction in the tangential direction.

Ultimate limit strength analysis of SPs subjected to external pressure and bending moment independently employs Riks method (the arc-length method) and automatic increment control (the load controlled Newton-Raphson method), respectively. Combined loading is initially implemented by fixed increments of external pressure, followed by incremental rotations until buckling failure is achieved. The external pressure is applied on the outer pipe through surface load. The

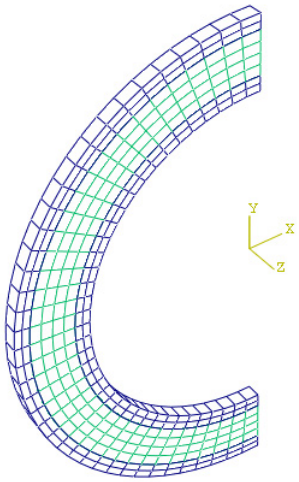

Figure 5. A schematic view of the finite element mesh for SPs.

bending moment is induced by defining the rotational displacement in the x-direction axis at the reference point located at the neutral axis. Automatically generated kinematic coupling equations are used to link the degrees of freedom of the nodes of the transverse plane to the reference point. The coupling of the translational freedom along the z-axis induces a plane strain state for the SPs section in order to simulate a long pipe configuration.

3. NUMERICAL EVALUATION AND PARAMETRIC STUDY

3.1 Numerical analysis of sandwich pipes under external pressure

By simulating the behavior of sandwich pipes under hydrostatic pressure, the collapse pressures (P_{co}) of the sandwich pipes filled with SFRC10, SFRC15 and SFRC20 are 40.22, 44.63 and 46.12 Mpa, respectively. The contour plots of the Von Mises stress and compressive damage field for SFRC10 at the collapse pressure are represented in Fig 6.

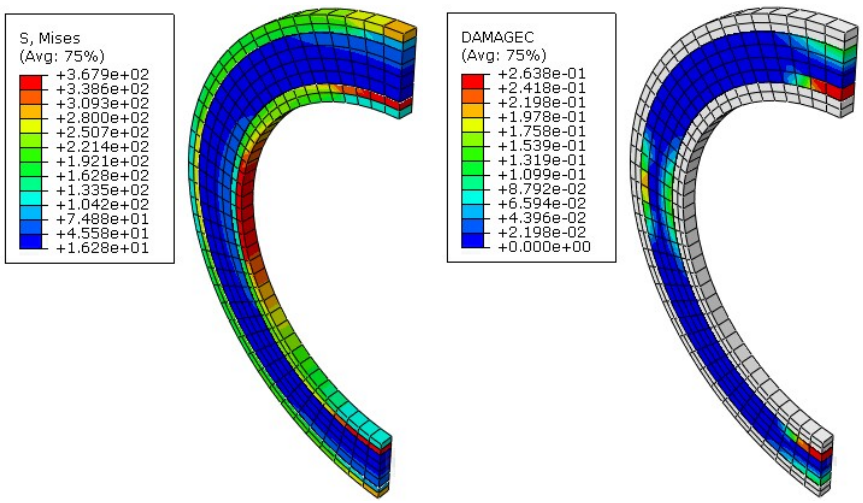

(a) Von Mises stress (b) Compressive damage

Figure 6. The contour plots of the Von Mises stress and compressive damage fields for SFRC10 at the collapse pressure

3.2 Numerical analysis of sandwich pipes under combined external pressure and bending

The limit strength analysis is performed for SPs under combined external pressure and bending. The pressure-curvature collapse envelopes for the analyzed SPs are shown in Fig. 7. Each envelope is described by six points, corresponding to constant pressure of 0%, 20%, 40%, 60%, 80% and 100% of the corresponding collapse pressure (P_{co}). The results of the Von Mises stress, compressive damage and tension damage for SFRC10 under the limit load are shown in Fig. 8, where the applied external pressure is 20% of the corresponding collapse pressure P_{co}. It can be seen that when

the collapse happens, the SFRC is almost completely damaged by compressive stress, while tensile damage is almost negligible.

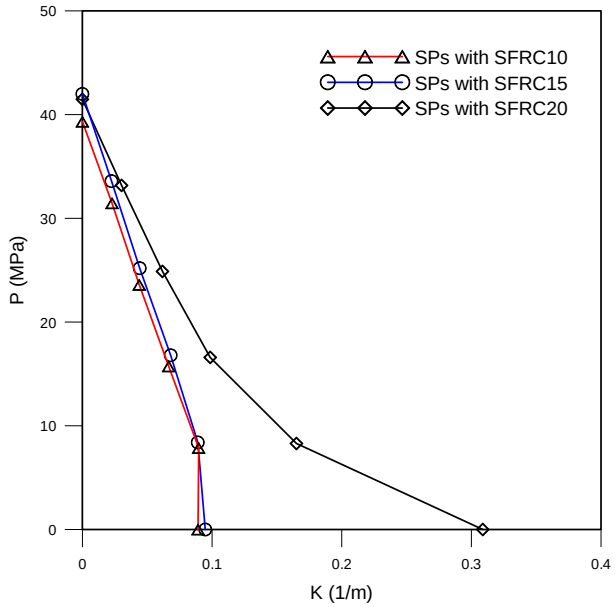

Figure 7. Pressure-curvature ultimate strength for SPs filled with different fiber-content SFRC

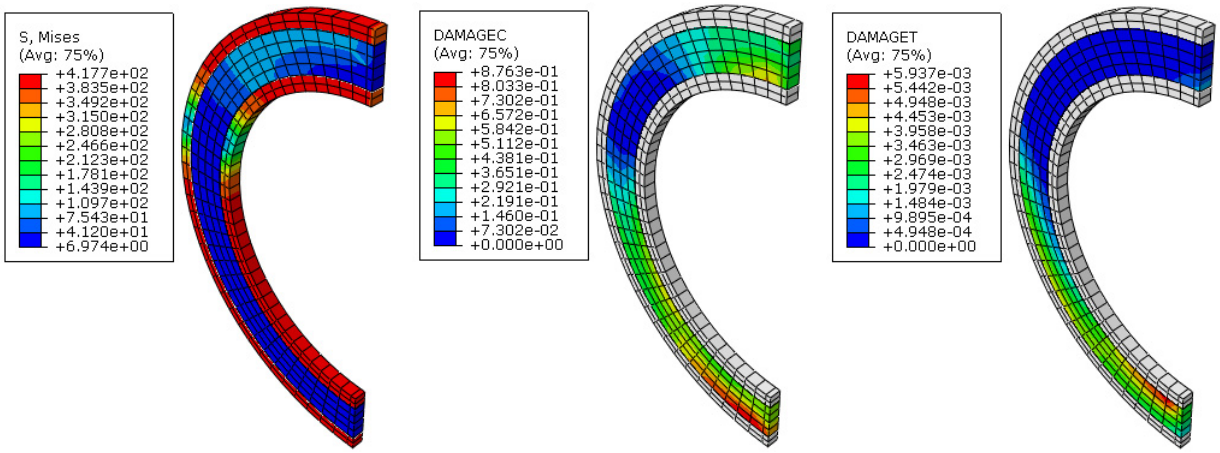

(a) Von Mises stress (b) Compressive damage (c) Tensile damage

Figure 8. The contour plots of the Von Mises stress, compressive damage and tension damage fields for SFRC10 under the limit load ($20\%P_{co}$ and bending)

3.3 Parametric analysis on the collapse pressure

To the different SPs possessing same internal diameter of the inner pipe, the thicknesses of the inner pipe t_i, the annulus t_a and the outer pipe t_e are the parameters affecting the ultimate strength under combined pressure and bending. For the parametric study, thicknesses t_i and t_e are assumed identical for simplicity and an initial out-of-roundness of 1% is considered. The geometric properties of the calculated SPs in case 1 and 2 are presented in Table 4, where D_{ni} and D_{ne} are the inner and outer nominal diameters, t_i and t_e the wall thicknesses. Fig. 9 shows the pressure-curvature collapse envelopes for the SPs with different thickness of the annulus t_a, and Fig. 10 shows the pressure-curvature collapse envelopes for the SPs with same inner and outer nominal diameters but different wall thickness. From the results, it can be observed that the collapse pressure of SPs under external pressure rises with the value of t_a increasing, while the variation of the collapse curvature of SPs under pure bending is not significant with t_a increasing. In addition, both the collapse pressure and collapse curvature of SPs under external pressure and pure bending, respectively, increase with the values of t_i and t_e increasing.

Table 4. Geometric properties of the calculated SPs

	D_{ni} (in)	t_i (mm)	D_{ne} (in)	t_e (mm)
Case 1				
SPs-1	6 5/8	6.35	8 5/8	6.35
SPs-2	6 5/8	6.35	10 3/4	6.35
Case 2				
SPs-3	6 5/8	4.78	8 5/8	4.78
SPs-4	6 5/8	6.35	8 5/8	6.35
SPs-5	6 5/8	8.74	8 5/8	8.74

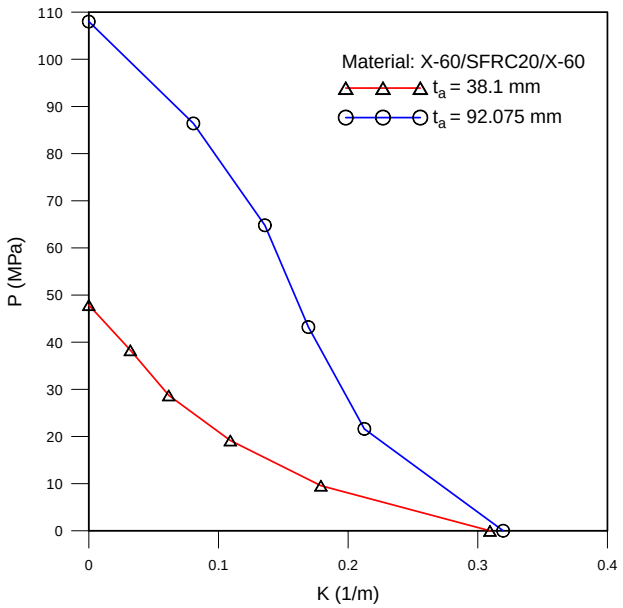

Figure 9. Pressure-curvature ultimate strength for SPs filled with SFRC20 for case 1 ($D_{ni} = 6\frac{5}{8}$ in, $t_i = t_e = 6.35$ mm).

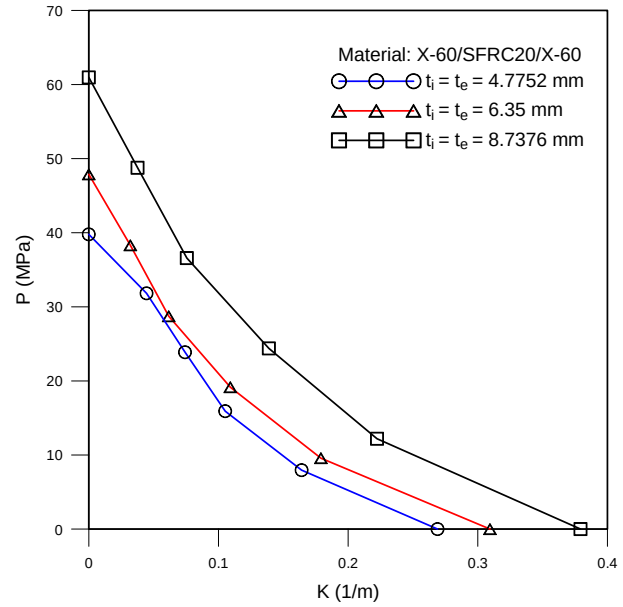

Figure 10. Pressure-curvature ultimate strength for SPs filled with SFRC20 for case 2 ($D_{ni} = 6\frac{5}{8}$ in, $D_{ne} = 8\frac{5}{8}$ in).

4. CONCLUSIONS

The SPs filled with SFRC are analyzed for ultimate strength under combined external pressure and bending, using a ring section model. To reduce the numerical instabilities due to the detection of cracks when using the smeared crack

concrete model, the material behavior of SFRC with different fiber content is modeled by damaged plasticity model in Abaqus 6.9-1, where the experimental data of the uniaxial compression and tension tests are adopted. The damage parameters are defined by the first-order decay exponential functions. Good agreement between experimental measurement and numerical analysis shows the accuracy of the proposed model for SFRC. The parametric study shows that the collapse pressure of SPs under external pressure increases with the annular thickness, while the collapse curvature of SPs under pure bending varies not significantly. Although the numerical results shows the preliminary feasibility of finite element modeling, further experimental studies are needed to verify the numerical models.

5. ACKNOWLEDGEMENTS

The authors acknowledge gratefully the financial support provided by CNPq, CAPES, FAPERJ and ANP of Brazil. C. An acknowledges gratefully the financial support provided by the China Scholarship Council. The authors are particularly grateful to Prof. Romildo D. Toledo Filho and Dr. Reila V. Velasco of Civil Engineering Program for sharing literature and experience on SFRC research. The advice on numerical modeling from Guangming Fu is also appreciated.

6. REFERENCES

ABAQUS/Standard, 6.9-1. *User's and Theory Manuals*. Hibbit, Karlsson and Sorensen, Inc.

Arjomandi, K. and Taheri, F., 2010. "Elastic buckling capacity of bonded and unbonded sandwich pipes under external hydrostatic pressure". *Journal of Mechanics of Materials and Structures*, Vol. 5, No. 3, pp. 391–408.

Arjomandi, K. and Taheri, F., 2011. "A new look at the external pressure capacity of sandwich pipes". *Marine Structures*.

Balaguru, P.N. and Shah, S.P., 1992. *Fiber-reinforced cement composites*. McGraw-Hill, New York.

Barth, K.E. and Wu, H.Y., 2006. "Efficient nonlinear finite element modeling of slab on steel stringer bridges". *Finite Elements in Analysis and Design*, Vol. 42, pp. 1304–1313.

Castello, X. and Estefen, S.F., 2007. "Limit strength and reeling effects of sandwich pipes with bonded layers". *International Journal of Mechanical Sciences*, Vol. 49, No. 5, pp. 577–588.

Castello, X. and Estefen, S.F., 2008. "Sandwich pipes for ultra deepwater applications". In *Proceedings of Offshore Technology Conference*. Houston, Texas, USA. OTC 19704.

Castello, X., Estefen, S.F., Leon, H.R., Chad, L.C. and Souza, J., 2009. "Design aspects and benefits of sandwich pipes for ultra deepwaters". In *Proceedings of the 28th International Conference on Ocean, Offshore and Arctic Engineering*. Honolulu, HI, USA. OMAE2009-79528.

Elchalakani, M., Zhao, X.L. and Grzebieta, R., 2002. "Tests on concrete filled double-skin (chs outer and shs inner) composite short columns under axial compression". *Thin-Walled Structures*, Vol. 40, No. 5, pp. 415–441.

Estefen, S.F., Netto, T.A. and Pasqualino, I.P., 2005. "Strength analyses of sandwich pipes for ultra deepwaters". *Journal of Applied Mechanics-Transactions of the Asme*, Vol. 72, No. 4, pp. 599–608.

Goode, C.D., Montague, P. and Nash, T., 1996. "Large reinforced concrete cylinders under external pressure". *Proceedings of the Institution of Civil Engineers-Structures and Buildings*, Vol. 116, No. 2, pp. 163–173.

Han, L.H., Huang, H. and Zhao, X.L., 2009. "Analytical behaviour of concrete-filled double skin steel tubular (cfdst) beam-columns under cyclic loading". *Thin-Walled Structures*, Vol. 47, No. 6-7, pp. 668–680.

Han, L.H., Tao, Z., Huang, H. and Zhao, X.L., 2004. "Concrete-filled double skin (shs outer and chs inner) steel tubular beam-columns". *Thin-Walled Structures*, Vol. 42, No. 9, pp. 1329–1355.

Han, L.H., Yao, G.H. and Tao, Z., 2007. "Performance of concrete-filled thin-walled steel tubes under pure torsion". *Thin-Walled Structures*, Vol. 45, No. 1, pp. 24–36.

Holschemacher, K., Mueller, T. and Ribakov, Y., 2010. "Effect of steel fibres on mechanical properties of high-strength concrete". *Materials & Design*, Vol. 31, No. 5, pp. 2604–2615.

Huang, H., Han, L.H., Tao, Z. and Zhao, X.L., 2010. "Analytical behaviour of concrete-filled double skin steel tubular (cfdst) stub columns". *Journal of Constructional Steel Research*, Vol. 66, No. 4, pp. 542–555.

Kim, T.S. and Kuwamura, H., 2007. "Finite element modeling of bolted connections in thin-walled stainless steel plates under static shear". *Thin-Walled Structures*, Vol. 45, No. 4, pp. 407–421.

Lu, X.B. and Hsu, C.T.T., 2006. "Behavior of high strength concrete with and without steel fiber reinforcement in triaxial compression". *Cement and Concrete Research*, Vol. 36, No. 9, pp. 1679–1685.

Montague, P., 1978. "Experimental behavior of double-skinned, composite, circular cylindrical-shells under external-pressure". *Journal of Mechanical Engineering Science*, Vol. 20, No. 1, pp. 21–34.

Su, J., Cerqueira, D.R. and Estefen, S.F., 2005. "Simulation of transient heat transfer of sandwich pipes with active electrical heating". *Journal of Offshore Mechanics and Arctic Engineering-Transactions of the Asme*, Vol. 127, No. 4, pp. 366–370.

Tao, Z., Han, L.H. and Zhao, X.L., 2004. "Behaviour of concrete-filled double skin (chs inner and chs outer) steel tubular stub columns and beam-columns". *Journal of Constructional Steel Research*, Vol. 60, No. 8, pp. 1129–1158.

Thomas, J. and Ramaswamy, A., 2007. "Mechanical properties of steel fiber-reinforced concrete". *Journal of Materials*

in Civil Engineering, Vol. 19, No. 5, pp. 385–392.

Velasco, R.V., 2008. *Self-consolidating concretes reinforced with high volumetrics fracions of steel fibers: rheological, physics, mechanics and thermal properties*. Ph.D. thesis, COPPE, Federal University of Rio de Janeiro, Rio de Janeiro.

Wang, J.C. and Chen, Y.K., 2006. *Application of ABAQUS in Civil Engineering*. Zhejiang University Press, Hangzhou, P. R. China.

Wei, S., Mau, S.T., Vipulanandan, C. and Mantrala, S.K., 1995a. "Performance of new sandwich tube under axial loading - analysis". *Journal of Structural Engineering-Asce*, Vol. 121, No. 12, pp. 1815–1821.

Wei, S., Mau, S.T., Vipulanandan, C. and Mantrala, S.K., 1995b. "Performance of new sandwich tube under axial loading - experiment". *Journal of Structural Engineering-Asce*, Vol. 121, No. 12, pp. 1806–1814.

Wright, H.D., Oduyemi, T.O.S. and Evans, H.R., 1991a. "The design of double skin composite elements". *Journal of Constructional Steel Research*, Vol. 19, No. 2, pp. 111–132.

Wright, H.D., Oduyemi, T.O.S. and Evans, H.R., 1991b. "The experimental behavior of double skin composite elements". *Journal of Constructional Steel Research*, Vol. 19, No. 2, pp. 97–110.

Yagishita, F., Kitoh, H., Sugimoto, M., Tanihira, T. and Sonoda, K., 2000. "Double-skin composite tubular columns subjected cyclic horizontal force and constant axial force". In *Proceedings of the Sixth ASCCS Conference*. Los Angeles, USA, Vol. 1, pp. 497–503.

Yu, T., Teng, J.G., Wong, Y.L. and Dong, S.L., 2010a. "Finite element modeling of confined concrete-i: Drucker-prager type plasticity model". *Engineering Structures*, Vol. 32, No. 3, pp. 665–679.

Yu, T., Teng, J.G., Wong, Y.L. and Dong, S.L., 2010b. "Finite element modeling of confined concrete-ii: Plastic-damage model". *Engineering Structures*, Vol. 32, No. 3, pp. 680–691.

Zhao, X.L., Han, B.K. and Grzebieta, R.H., 2002. "Plastic mechanism analysis of concrete-filled double-skin (shs inner and shs outer) stub columns". *Thin-Walled Structures*, Vol. 40, No. 10, pp. 815–833.